AIP Advances

^{241}Am/Be source optimum geometry for DSRS management-based Monte Carlo simulations

Cite as: AIP Advances **11**, 115024 (2021); https://doi.org/10.1063/5.0063005
Submitted: 10 July 2021 • Accepted: 13 September 2021 • Published Online: 17 November 2021

Cebastien Joel Guembou Shouop, Maurice Ndontchueng Moyo, Eric Jilbert Nguelem Mekongtso, et al.

^{241}Am/Be source optimum geometry for DSRS management-based Monte Carlo simulations

Cite as: AIP Advances 11, 115024 (2021); doi: 10.1063/5.0063005
Submitted: 10 July 2021 • Accepted: 13 September 2021 •
Published Online: 17 November 2021

Cebastien Joel Guembou Shouop,[1,2,a)] Maurice Ndontchueng Moyo,[1,2] Eric Jilbert Nguelem Mekongtso,[1,2] Jean Felix Beyala Ateba,[2] and David Strivay[3]

AFFILIATIONS

[1] UFD Mathématiques, Informatique Appliquée et Physique Fondamentale, Université de Douala, P.O. Box 24157, Douala, Cameroon
[2] National Radiation Protection Agency of Cameroon, P.O. Box 33732, Yaounde, Cameroon
[3] Atomic and Nuclear Spectroscopy, Archeometry, University of Liège, Bat. B15 Sart Tilman, 4000 Liege 1, Belgium

[a)] **Author to whom correspondence should be addressed:** sebastianguembou@gmail.com

ABSTRACT

The geometry form related to ^{241}Am/Be spontaneous neutron sources has been investigated to evaluate the most optimizing geometry for disused sealed radioactive source (DSRS) disposal. Nine source geometries were assessed: point, disk, sphere 1, sphere 2, sphere 3, cylinder 1, cylinder 2, rectangle 1, and rectangle 2. The most radiological optimizing geometries were found to be the disk, followed by the point source, sphere 1, and cylinder 1, while the rectangle or parallelepiped 2 source forms were the worst cases. Neutron and photon generated fluxes were computed, and the parallelepiped 2 source geometry generated the lower value of flux inversely to the effective dose rate computed in the decision-making area, where it was found to be the highest value. The obtained results were in agreement with the as low as reasonably achievable principle for the exposure rate optimization. The obtained exposure dose rates were found to be <~2 μSv/h (maximum value on horizontal calculation) and 1.75 μSv/h (maximum value on vertical computation), which are lower than the 2.5 μSv/h acceptable limit for the public area. Whenever possible, the DSRSs should be pressed into a disk form (or a cylindrical form with a small height) before embedding them into the Am1 P60 capsule for disposal purposes. The dose profile for the ^{241}Am/Be source obtained, the neutron flux, and the gamma generated from neutron absorption showed agreement with the expected experimental physical data. The supported data contribute to postulate that Monte Carlo methods are effective computational tools that can be used to select the most effective radioactive waste form for disposal purposes.

I. INTRODUCTION

In recent decades, industrial and medical applications involving the use of radiation sources have been spreading all over the world. Gamma and neutron sources are seen to be the most preferable radiation sources used in many of these practices, such as radiography, radiology, and energy development. According to radiation protection principles, manufacturing of these radioactive sources requires geometry optimization in view of minimizing self-absorption. To this extent, point-like and disk geometries have proven to be more adequate and economic than other geometry forms.

However, if these sealed radiation sources after being used cannot be recycled or reused for another purpose, they become "disused radioactive sources." Safe management of these disused radioactive sources has been a great concern worldwide. This is because the safe management of these sources requires dismantle and disposal in appropriate geometry forms in view of minimizing external radiation exposure. The present study is thereby to investigate the optimizing geometry among the point-like source, disk source, spherical source, cylindrical source, and rectangular or parallelepiped solid available to be used for the disposal of ^{241}Am/Be neutron sources. To this extent, the PHITS (Particle and Heavy Ion Transport code System) Monte Carlo computer code was used to compute fluxes and radiation dose rates generated by neutron and gamma radiation from ^{241}Am/Be sources considered as disused sealed radioactive sources (DSRSs) to be disposed of.

II. MATERIAL AND METHODS

The present study uses the PHITS Monte Carlo code to assess the most optimizing geometry for DSRSs' disposal at their end-life cycle. The description of the investigated geometry is given, and the computer methods are presented afterward.

A. Geometry of the DSRS package

The investigated geometry forms together with their characteristics are presented in Table I, which are the point-like source (a single identifiable localized source of ^{241}Am/Be), disk source (which is plated on the surface of a disk and the active area is the surface of the disk), spherical source (uniformly distributed in a sphere), cylindrical source, and rectangular or parallelepiped solid. Since disused sealed radioactive sources (DSRSs) are to be disposed of in P60 capsules, the internal radius of the Am1 P60 capsule allows us to store up to three spherical sources in the dedicated area. This is the reason why it is important to assess the capacity of the above-mentioned geometry form available to be used for radioactive source disposal as depicted in Table I and Fig. 1.

B. Monte Carlo simulation

Monte Carlo (MC) techniques are considered as a subset of computational algorithms that utilize the process of repeated random sampling to numerically estimate unknown parameters.[1–4] They are used to model complex situations and problems with a high degree of freedom that cannot be analytically solved by generating random numbers and random experiments.[5–7] The use of Monte Carlo to evaluate the most appropriate geometry form container to be used to store ^{241}Am/Be DSRSs for disposal is mainly based on the source strength while escaping a specific geometry.[5–9] The source strength can be evaluated by computing its neutron flux escaping the geometry and the effective dose rate from the enclosed geometry. The tally set for the ^{241}Am/Be neutron source is 101 and that of the enclosure area for operators of the facility is 104. 102 and 103 are the intermediate tallies for the DSRS packages in other to handle them easily and to shield neutron spontaneously emitted and gamma ray generated from neutron absorption and interaction.

C. The PHITS input code

The Particle and Heavy Ion Transport code System (PHITS) was used for simulation in the present research. It is a general-purpose Monte Carlo system based on the Fortran code.[10–18] The PHITS version 3.22 was used for computation, including simulation of photons and neutrons in a wide range of energy. The PHITS code was used to validate the model developed in the present study and to verify the shielding effectiveness of the ^{241}Am/Be DSRS source "containers."[10,13,14] The PHITS code used for neutron source and geometry simulation, neutron and gamma flux calculations, and radiation protection requires proper material definition and geometry construction following a clear and well-defined method. The parameter set for uncertainty calculation in the present project was based on the following equation implemented by the PHITS research team:[5,10,11,13,14,19–27]

$$\sigma = \sqrt{\frac{\sum_{i=1}^{N}\left(x_i w_i \Big/ \overline{w}\right)^2 - N\overline{X}^2}{N(N-1)}}. \quad (1)$$

The PHITS input code was executed using the radioactive decay process; a data library from DECDC2 (Nuclear DECay Data for Dosimetry Calculation, Version 2) revised data from ICRP Publication 38.[28,29] The multiplier sections used dose conversion

TABLE I. Different types of geometries used for dismantled DSRS form or manufactured: influence on source safe conditioning as DSRS Am-242/Be (323 mCi): Geometry, volume, and external surface.

Geometry type for waste conditioning	Dimensions	Geometrical form	Volume (cm^3)	External surface (cm^2)
Point-like source (r = ~0)	Point (x_0, y_0, z_0)		~0	~0
Disk source (r = 2.7, h = ~0)	Radius r Center (x_0, y_0)		~0	~πr = (22.9)
Spherical source (r = 2.7) and (n = 1, 2, 3)	Radius r Center (x_0, y_0, z_0)	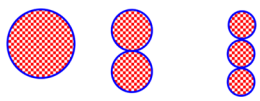	$4\pi r^3/3$ = (82.45), (164.9), and (247.35)	$4\pi r^2$ = (91.61), (183.22), and (274.83)
Finite cylindrical source (r = 2.7, h = 10) and (r = 2.7, h = 20)	Radius r Height h Center of the bottom face (x_0, y_0, z_0)	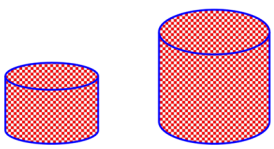	πhr^2 = (229.02) and (458.04)	$2\pi r(h + r)$ = (215.45) and (385.1)
Rectangular or parallelepiped source (x = y, z) = (1.16, 1.16, 10) and (1.16, 1.16, 20)	Thickness X×Y×X x_{min}, x_{max} y_{min}, y_{max} z_{min}, z_{max}	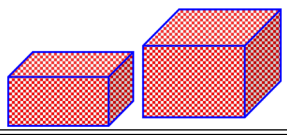	x · y · z = (13.5) and (27)	2(x · y + x · z + y · z) = (49.18) and (95.65)

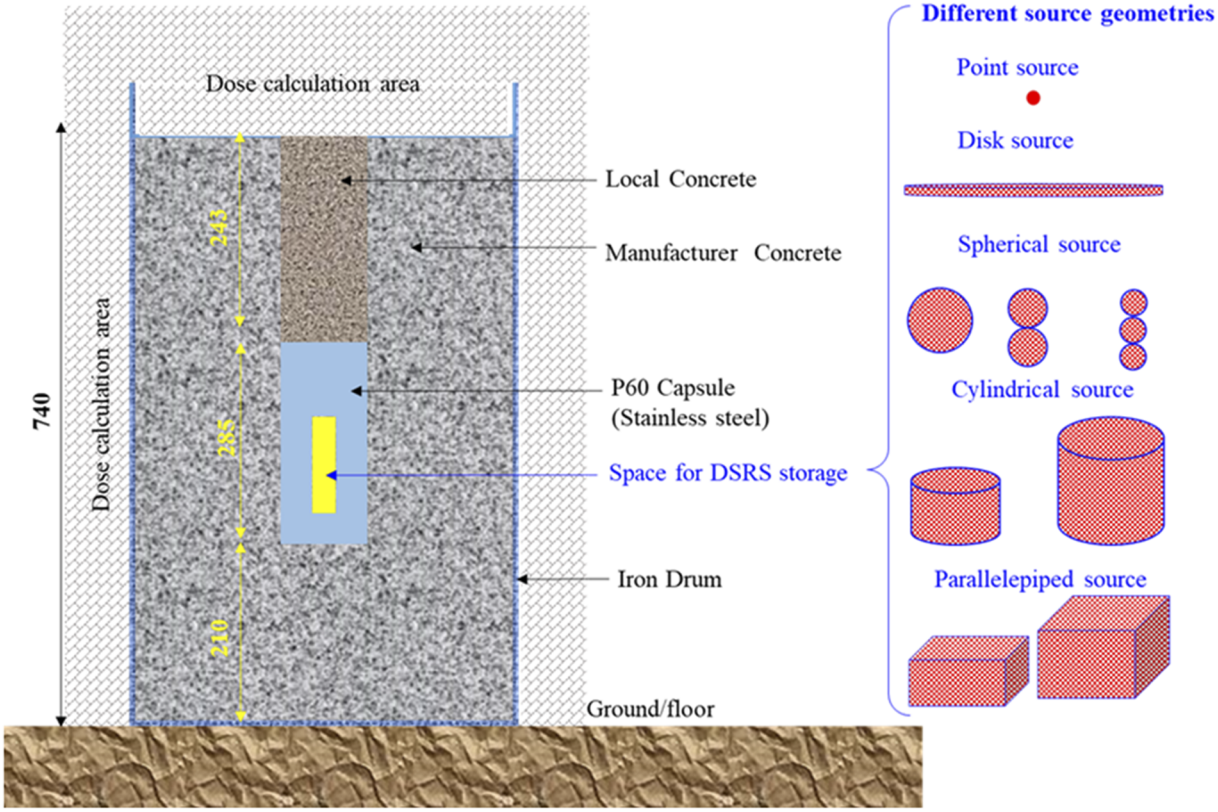

FIG. 1. Geometry of the simulation designed for DSRSs, made of an ^{241}Am/Be neutron source. The fluxes were computed at crossing surfaces between different cells, and the effective dose calculation area is set on the r-axis (referred to as the x-axis or horizontal axis) and z-axis (referred to as the vertical axis in the remaining part of the manuscript).

coefficients for neutrons and photons from ICRP116. This library has been compiled for 1034 radionuclides for dose calculation in medical, environmental, and occupational exposures. It is a library built from the assembled set of Evaluated Nuclear Structure Data File (ENSDF).[11,20,24,30,31] Since neutron interaction with a medium generates gamma-ray emission, the weighted summation of the tally result is calculated by the following equation:

$$\overline{X} = F\sum_{j=1}^{N} \frac{r_j}{r}\overline{X}_j, \tag{2}$$

where F is the normalization factor defined by the *sumfactor*, N is the number of summing up files by *nfile*, $\overline{X}_j$ is the jth tally result, r_j is the weighted value of the jth tally, and r is the sum of r_j,

$$r = \sum_{j=1}^{N} r_j. \tag{3}$$

The uncertainty of the summation, σ_X, can be calculated by the following equation:

$$\sigma_X = F\sqrt{\sum_{j=1}^{N}\left(\frac{r_j}{r}\right)^2 \sigma_{\overline{X}_j}^2}, \tag{4}$$

where $\sigma_{\overline{X}_j}^2$ is the standard deviation of the jth tally result.

The PHITS Monte Carlo input code for the present study includes the following sections: Title, Parameters, Source, Material, MatNameColor, Surface, Cell, T-3Dshow, Importance, 03 T-Track sections, Multiplier, and End.[11,21,22,32] The T-Track section defines different physical values that should be extracted during the simulation in order to discuss the obtained data.

D. ^{241}Am/Be neutron source simulated

The DSRS consisted of an isotropic (α, n) ^{241}Am/Be neutron source. The source activity at the time of simulation was 321.82 Bq as reported at the centralized temporary waste management facility. The α-emitter is Am-241, the target is Be-9, the Q-value of the reaction is 5.71 MeV, and the neutron yield per α is ~7.0×10^{-5} for the following reaction:[33]

$$\begin{gathered} {}^{238}_{92}U + {}^{4}_{2}He \rightarrow {}^{241}_{94}Pu + {}^{1}_{0}n, \\ {}^{241}_{94}Pu \xrightarrow{\beta^-} {}^{241}_{95}Am. \end{gathered} \tag{5}$$

The source definition was done in PHITS input code using ispfs (1) for spontaneous fissions in all directions. A volume source (cylindrical) was defined inside the P60 capsule prepared to contain the

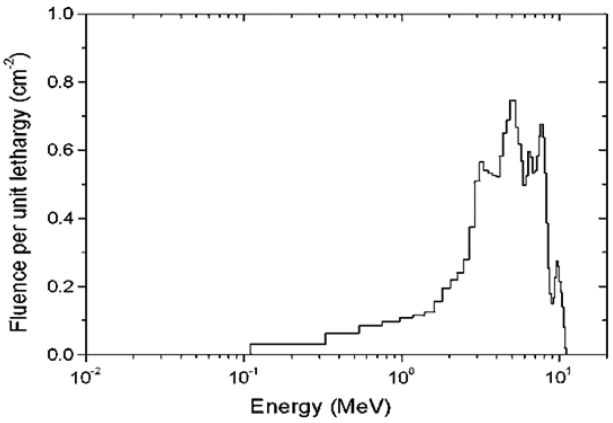

FIG. 2. ^{241}Am/Be neutron spectrum from ISO 8529 used for Monte Carlo simulation. The source strength depends on the normalized spectra given here.

dismantled DSRSs. The energy spectrum of the ^{241}Am/Be source used is shown in Fig. 2. Regarding the neutron emission rate, Leddicottee[34] measured an emission rate of 5.7×10^6 n/s in 1962. In 2019, Tohamy *et al.* in their study expected a neutron yield of $(2.2 \pm 0.2) \times 10^6$ s^{-1} Ci^{-1}.[35–39] These details were implemented for the source definition in the present study using neutrons with a mean energy of 4.5 MeV in association with 4.438 MeV γ-rays according to the reaction ^{241}Am (n, γ)^{12}C.

III. RESULTS AND DISCUSSIONS

The normalized neutron and photon fluxes are shown in Figs. 3 and 4. The neutron flux is higher at the ^{241}Am/Be source position, which is confined in the Am1 P60 capsule. The remaining space in the P60 capsule is filled with air in the simulated model. The neutron flux is symmetric to the z-axis, and the neutron attenuation by the geometry decreases quickly from inside to outside. Photon flux is comparably hotter in the middle, being about one order of

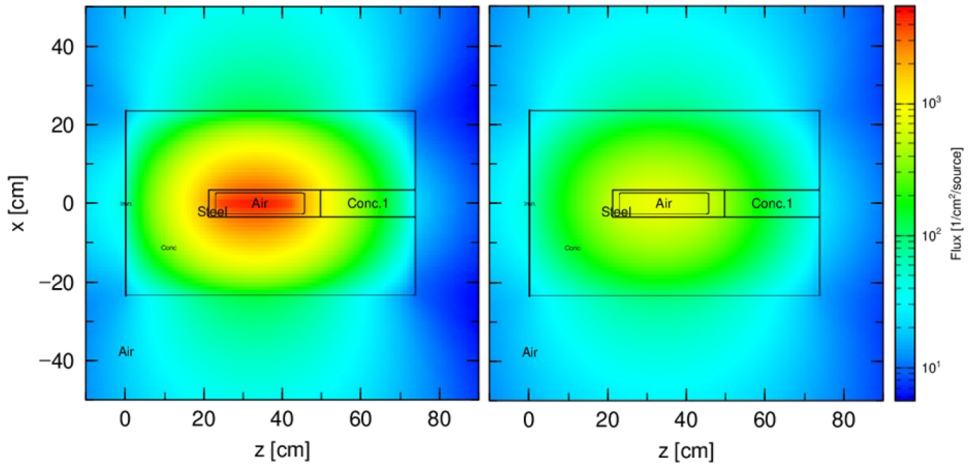

FIG. 3. Neutron and gamma fluxes from the ^{241}Am/Be source in the form of rectangle 2 or parallelepiped (less optimizing source geometry).

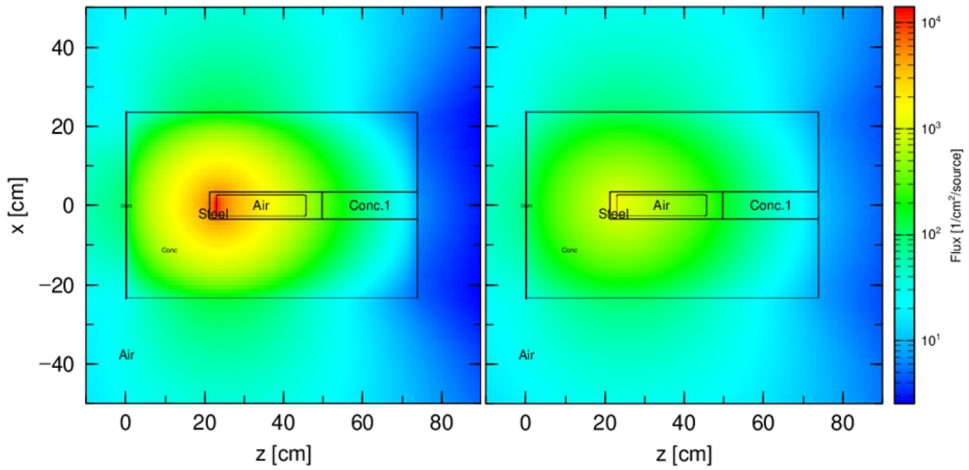

FIG. 4. Neutron and gamma fluxes from the ^{241}Am/Be source in the disk geometry (best option for the source geometry optimization).

magnitude less than that of neutrons. However, when neutrons undergo total absorption, the photon fluxes increase significantly to be higher than the neutron flux in the areas set for effective dose calculation. This is achieved by comparing the top (z-axis) of the geometry where the dark blue color represents the lowest flux and the red color in the center of the geometry represents the maximum flux. This is the main reason why neutron shielding always involved gamma shielding material set at a position where the neutron absorption reaches its paroxysm. This can be observed at the position (x; z) = ([−50 +50]; [80 90]) in the unit of cm.

Comparison of the neutron fluxes from parallelepiped and disk sources was carried out as shown in Figs. 3 and 4. It can be observed that the neutron parallelepiped source form displays a spread out flux, while the disk source form presents a focused flux. While the spread out flux is even larger than the focused one inside the capsule, it can be seen in Table II that the primary neutron flux exiting out the source cell is smaller for the rectangle 1 form ($1.5022 \times 10^6 \pm 0.0009$ n cm^{-2}) and larger for the point source ($1.6223 \times 10^6 \pm 0.0008$ n cm^{-2}) and the disk source ($1.5966 \times 10^6 \pm 0.0008$ n cm^{-2}). The comparison of the total neutron flux exiting out the geometry, including secondary neutrons (calculated in the area set for the effective dose calculation—Fig. 1), in different geometries shows that the flux is higher for the disk geometry while it is lower for the rectangle 2 geometry with the value of $1.6648 \times 10^6 \pm 0.0006$ and $1.5860 \times 10^6 \pm 0.0006$ n cm^{-2}, respectively.

Table III shows the effective dose rate calculated at contact and at 1 m away from the DSRS container. In contact with horizontal (x-axis), on top of Z (z-axis), at 1 m away from horizontal (x-axis), and at 1 m away from vertical (z-axis), the estimated values of the effective dose rate showed that the best optimizing source geometry is disk geometry, followed by the point source, sphere source, cylinder 1, sphere 2, cylinder 2, rectangle 1, and sphere 3. The less optimizing source geometry was found to be rectangle 2. The results can be seen in Figs. 5–9 where the plotted graphs display the effective dose rate in the geometry and the surrounding areas.

The comparison made with the neutron flux as discussed above seems to be contradictory as the higher the neutron flux, the lower the effective dose rate. However, there is no contradiction as the neutron flux from the disk source is likely to travel a larger distance before escaping the geometry, while the neutron flux emitted from the surface of the source in the parallelepiped form is likely to travel the smallest distance before reaching the cell or tally set for radiation dose calculation. This means that energetic neutrons are likely to exit the geometry and account for the dose calculation in the rectangle-2 source, while they are thermalized in the disk geometry. In addition, the calculated effective dose displayed in Figs. 5–9 that accounts for the contribution of neutrons and gamma rays generated is higher when neutrons interact in the latter geometry and lower when neutrons undergo absorption quickly.

To evaluate the effectiveness of the geometry of the DSRS package, the dose profile was plotted for the decision-making process. It can be seen in Figs. 5–7 that the horizontal effective dose profiles up to ~4.5 m around the DSRS drum are displayed for each source geometry packed in the capsule. From these figures, it is observed that the distance needed to reduce the effective dose rate up to the as low as reasonably achievable (ALARA) acceptable limit for the public area (2.5 μSv/h) varies from 78.30 to 84.30 cm. It appears to

TABLE II. Neutron flux crossing different regions in the simulated geometry based on PHITS Monte Carlo. The crossing surfaces are made of areas between cells 100 and 101, 101 and 102, 102 and 103, and 103 and 104 (including secondary or scattered neutrons).

Region	Neutron flux crossing two region (n cm^{-2})								
	Point-like	Disk source	Sphere 1	Sphere 2	Sphere 3	Cylinder 1	Cylinder 2	Rectangle 1	Rectangle 2
100–101 (primary neutron flux from the source)	$1.6223 \times 10^6 \pm 0.0008$	$1.5966 \times 10^6 \pm 0.0008$	$1.5050 \times 10^6 \pm 0.0007$	$1.5511 \times 10^6 \pm 0.0006$	$1.5627 \times 10^6 \pm 0.0005$	$1.5622 \times 10^6 \pm 0.0012$	$1.5788 \times 10^6 \pm 0.0008$	$1.5022 \times 10^6 \pm 0.0009$	$1.5148 \times 10^6 \pm 0.0007$
101–102	$2.2168 \times 10^4 \pm 0.0036$	$2.1427 \times 10^4 \pm 0.0045$	$2.4148 \times 10^4 \pm 0.0037$	$3.5595 \times 10^4 \pm 0.0027$	$4.8361 \times 10^4 \pm 0.0047$	$3.2519 \times 10^4 \pm 0.0038$	$5.4871 \times 10^4 \pm 0.0030$	$3.2476 \times 10^4 \pm 0.0032$	$5.4529 \times 10^4 \pm 0.0026$
102–103	$9.0984 \times 10^4 \pm 0.0027$	$8.8179 \times 10^4 \pm 0.0033$	$1.0020 \times 10^5 \pm 0.0022$	$1.4893 \times 10^5 \pm 0.0006$	$2.0241 \times 10^5 \pm 0.0021$	$1.3439 \times 10^5 \pm 0.0024$	$2.2765 \times 10^5 \pm 0.0020$	$1.3537 \times 10^5 \pm 0.0024$	$2.2818 \times 10^5 \pm 0.0009$
103–104 (total neutron flux exiting the geometry, including secondary neutrons)	$1.6613 \times 10^6 \pm 0.0003$	$1.6648 \times 10^6 \pm 0.0006$	$1.6440 \times 10^6 \pm 0.0005$	$1.6178 \times 10^6 \pm 0.0005$	$1.5980 \times 10^6 \pm 0.0007$	$1.6240 \times 10^6 \pm 0.0005$	$1.5909 \times 10^6 \pm 0.0004$	$1.6201 \times 10^6 \pm 0.0006$	$1.5860 \times 10^6 \pm 0.0006$

TABLE III. Effective dose rate for the decision-making process based on Monte Carlo simulation in view of achieving public exposure condition in the boundary adjacent areas to the DSRS container. Public exposure here refers to the ALARA principle of less than 1 mSv/year, which in other words means 2.5 μSv/h.

	Effective dose at different positions (μSv/h)			
Geometry	In contact with horizontal (x-axis)	Contact on top of Z (z-axis)	1 m away from horizontal (x-axis)	1 m away from vertical (z-axis)
Point-like	3.04×10^{1}	1.29×10^{0}	1.72×10^{0}	1.11×10^{-1}
Disk source	3.03×10^{1}	1.24×10^{0}	1.70×10^{0}	1.05×10^{-1}
Sphere 1	3.24×10^{1}	1.49×10^{0}	1.81×10^{0}	1.18×10^{-1}
Sphere 2	3.41×10^{1}	2.45×10^{0}	1.87×10^{0}	1.75×10^{-1}
Sphere 3	3.44×10^{1}	3.77×10^{0}	1.88×10^{0}	2.40×10^{-1}
Cylinder 1	3.37×10^{1}	2.13×10^{0}	1.84×10^{0}	1.59×10^{-1}
Cylinder 2	3.42×10^{1}	4.41×10^{0}	1.85×10^{0}	2.85×10^{-1}
Rectangle 1	3.42×10^{1}	2.22×10^{0}	1.86×10^{0}	1.61×10^{-1}
Rectangle 2	3.48×10^{1}	4.60×10^{0}	1.89×10^{0}	2.92×10^{-1}
Minimizing geometry	Disk source			
Maximizing geometry	Rectangle 2			

be from 102.00 to 108.00 cm, as displayed in Fig. 6, but the radius of the container is 23.70 cm. These results are in accordance with the international atomic energy agency regulations (IAEA) for the waste drum design. The decrease in the effective dose displayed in Fig. 7 shows its value in the closest 1 m from the surface of the DSRS container. It can be concluded that the design is effective as the effective dose rate at 1 m from the contact of the DSRS container is <~2 μSv/h. Thus, containing the dismantled DSRSs in an Am P60 capsule, sealing, and disposal activities could now be implemented at the centralized disused sealed radioactive source storage.

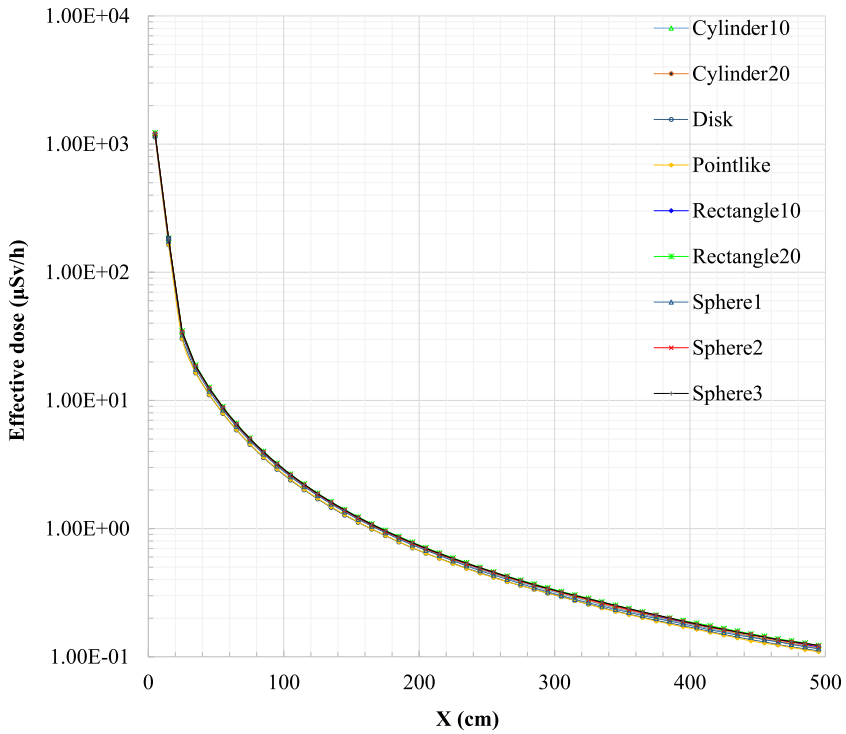

FIG. 5. Effective dose (horizontal profile or x-axis) investigated from the tally for output results where the interval 0–23.7 cm represents the DSRS container radius and the interval 23.7–500 cm corresponds to the closest area to the encapsulated waste to be disposed of.

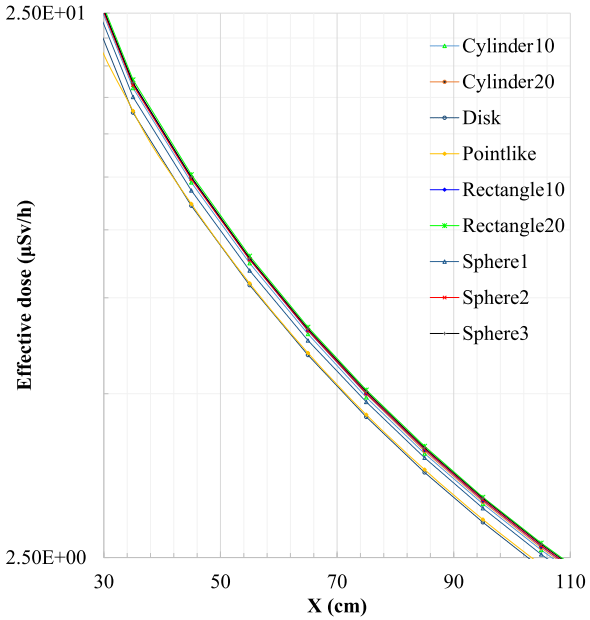

FIG. 6. Effective dose evolution inside the DSRS container (from 0 to 23.5 cm) and in the closest horizontal boundary area to reach the ALARA acceptable dose limit of 2.5 μSv/h for the public acceptance.

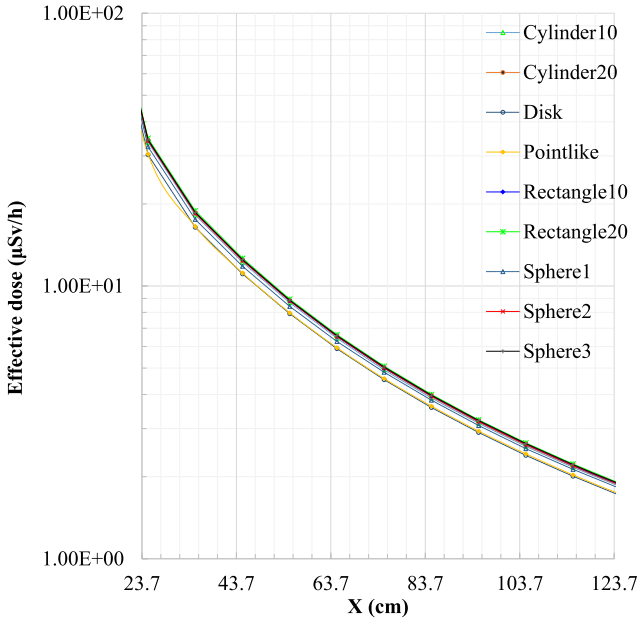

FIG. 7. Dose evolution from the DSRS container's contact point to 1 m away. The effective dose drops from 33.3 ± 0.0014 μSv/h at contact to 1.75 ± 0.0041 μSv/h at 1 m, which is acceptable for the ALARA hypothesis.

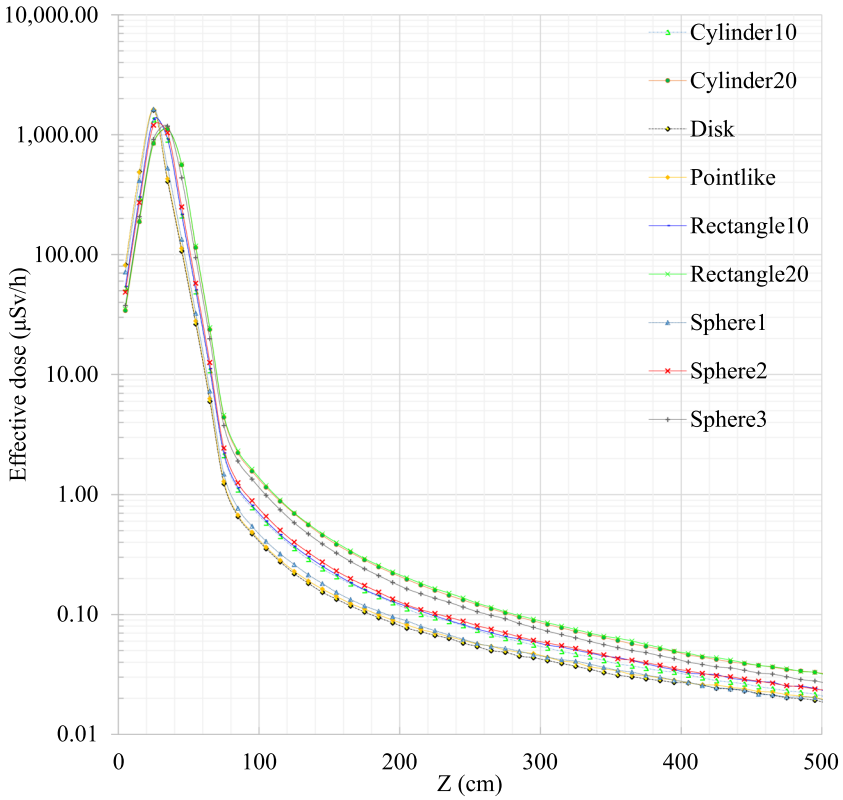

FIG. 8. Effective dose (vertical profile or z-axis) investigated from the tally for output results where the interval 0–74 cm represents the DSRS container height and the interval 74–1000 cm corresponds to the closest area on top of the encapsulated waste to be disposed of.

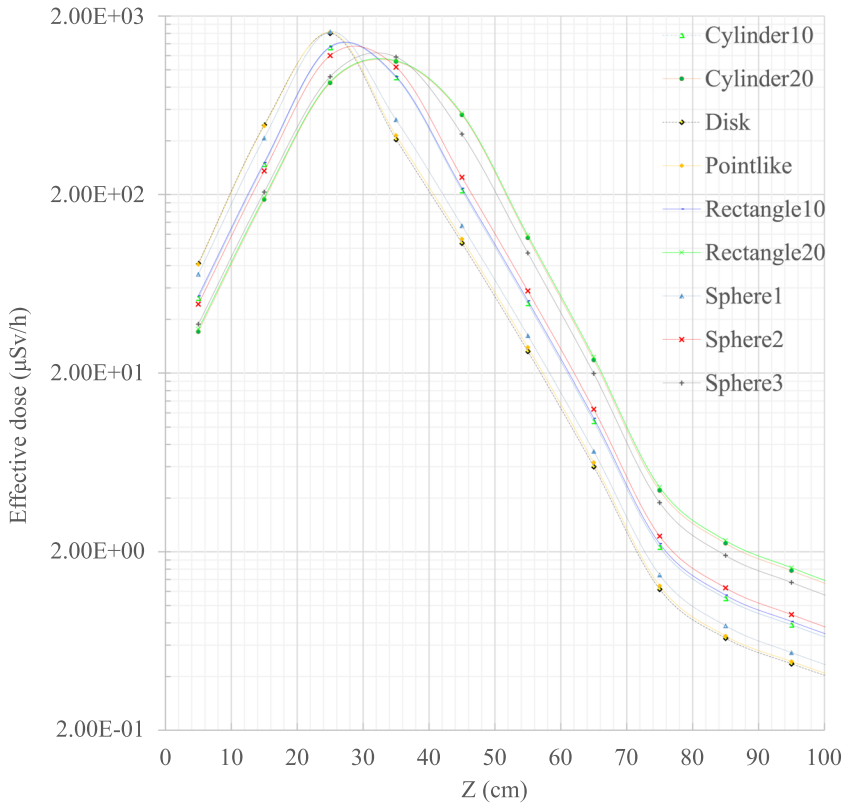

FIG. 9. Effective dose profile inside the DSRS container (from 0 to 74 cm) where the position of the ^{241}Am/Be source pre-encased in a P60 capsule encapsulated into the concrete-filled drum is set between 21.2 and 49.7 cm.

This could be achieved by taking into consideration the best optimizing source geometry of the disk, followed by the point source, sphere 1, cylinder 1, sphere 2, cylinder 2, rectangle 1, sphere 3, and finally parallelepiped 2 or rectangle 2 (the worst case). It is important to notice that the effective solutions are sphere 1 and cylinders 1 and 2 as they allow making volumetric sources, the only way to dismantle and pack the ^{241}Am/Be DSRSs.

Figures 8 and 9 display the vertical effective dose profile. The definition of the source between 21.2 and 49.7 cm is the main reason why the maximum (a pick) is observed in this interval. The small shift on the top is due to the source geometry, which is not centralized on the Z-axis as observed in point, disk, and volume sources. While considering the ALARA principle, the effective dose rate at the contact of the top of the DSRS container varies from 0.45 (for disk geometry) to 1.75 μSv/h (for parallelepiped 2). These values are comparably lower than the regulatory value of 2.5 μSv/h set for public adjacent areas. The effective dose rate at 1 m from the top (z-axis) varies from 0.075 (for disk geometry) to 0.137 μSv/h (for parallelepiped 2), which is within the acceptable limit for the radiological safety of the public area.

IV. CONCLUSIONS

The optimum geometry of the ^{241}Am/Be disused sources based on PHITS Monte Carlo simulations for the disposal of DSRSs as a waste package was performed. The following source geometries were investigated: point, disk, sphere 1, sphere 2, sphere 3, cylinder 1, cylinder 2, rectangle 1, and rectangle 2. Among the investigated source geometries, the disk and point sources were found to generate the highest neutron flux at the exit of the DSRS capsule and disposal package, while the parallelepiped geometry generated the lowest flux. Inversely, the effective dose rate was higher for the rectangular 2 geometry and lower for the disk source geometry. In order to determine the most radiological optimizing source for the dismantling and disposal of DSRSs in a safe and secured way, the radiation doses were computed. The obtained results allow the evaluation of the DSRS storage capacity as the effective dose rate calculated for the 321.82 Bq of ^{241}Am/Be spontaneous neutron source shows lower values than the permissible ALARA principle.

The obtained results for radiation dose rates were observed to be <~2 μSv/h (maximum value at the horizontal calculation) and 1.75 μSv/h (maximum value at the vertical computation), which are lower than the 2.5 μSv/h acceptable limit for an area defined as the public zone. Whenever possible, the DSRSs should be pressed into a disk form (or cylindrical form with a small height) prior to their embedding into the Am1 P60 capsule and their encapsulation into the borate concrete drum prepared for neutron emitter disposal purposes. The dose profile for the ^{241}Am/Be source obtained, the neutron flux, and the gamma generated from neutron absorption showed agreement with the literature and fit our expectations. In conclusion, the Monte Carlo tools were effectively used to demonstrate that the best optimizing volume geometries are disk, sphere 1, and cylinder 1. In addition, one can say that Monte Carlo methods are effective computational tools that can be used to enhance

the "cradle to grave" management of disused radioactive sources. As the issue of nuclear waste management is an up-to-date topic, the future perspective will consist of looking at a Monte Carlo-based method (with statistic) to validate the most optimizing complex source geometry and the function of gamma, beta, and alpha sources.[41]

Monte Carlo simulation is a study to be done prior to the dismantling operation that enhances the cradle-to-grave management of DSRSs in developing countries, such as Cameroon. The dismantling operation could be undertaken at any time knowing that the best optimizing geometries are disk, sphere 1, cylinder 1, and cylinder 2 and that the effective dose rate in the enclosed areas to the DSRS container will remain less than the ALARA regulatory value of 2.5 μSv/h. In addition, another work should be performed to evaluate the safety and security of the disposal site and the interim storage in the condition where many DSRS drums are stored in several stages in a confined area. The present study also helped to evaluate the Am1 P60 capsule and the borate concrete-filled drum capacity of each developing country that has to deal with ^{241}Am/Be disused sources. A similar study is being carried out to evaluate the case of gamma emitter DSRSs, such as ^{137}Cs, ^{60}Co, and so on.[5,27,40]

ACKNOWLEDGMENTS

The authors are grateful to PHITS Collaboration (T. Sato, S. Hashimoto, and K. Niita *et al.*) for PHITS development. They want to extend their gratitude to the National Radiation Protection Agency of Cameroon (NRPA) for promoting Monte Carlo development in the research institute.

We confirm that the manuscript has been read and approved by all named authors and that there are no other persons who satisfied the criteria for authorship but are not listed. We further confirm that the order of authors listed in the manuscript has been approved by all of us. We confirm that we have given due consideration to the protection of intellectual property associated with this work and that there are no impediments to publication, including the timing of publication, with respect to intellectual property.

AUTHOR DECLARATIONS

Conflict of Interest

The authors have no conflicts to disclose.

Author contributions

All authors contributed equally to this work.

DATA AVAILABILITY

The data that support the findings of this study are available from the corresponding author upon reasonable request.

REFERENCES

[1]J. Baró, M. Roteta, J. M. Fernández-Varea, and F. Salvat, Radiat. Phys. Chem. **44**, 531 (1994).
[2]F. Salvat, J. Fernández-Varea, and J. Sempau, "PENELOPE, A code system for Monte Carlo simulation of electron and photon transport," in Workshop Proceedings, 2011.
[3]G. Zhang, *Monte Carlo Simulation of Mixed Neutron-Gamma Radiation Fields and Dosimetry Devices* (Elektrotechnik und Informationstechnik des Karlsruher Instituts für Technologie (KIT), 2011).
[4]A. M. Cantaragiu, C. Gheorghies, and C. Borcia, "Study of gamma spectra by Monte Carlo simulation," https://inis.iaea.org/collection/NCLCollectionStore/_Public/44/028/44028935.pdf.
[5]C. J. Guembou Shouop and B. Sang-In, Eur. Phys. J. Plus **135**, 784 (2020).
[6]G. Shouop, C. Joel, N. M. Maurice, N. Mekongtso, E. Jilbert, M. Ousmanou, and S. David, J. Environ. Radioact. **189**, 109 (2018).
[7]C. J. Guembou Shouop, S. I. Bak, M. Ndontchueng Moyo, E. J. Nguelem Mekongtso, and D. Strivay, AIP Adv. **10**, 075203 (2020).
[8]C. J. Guembou Shouop, M. Ndontchueng Moyo, E. J. Nguelem Mekongtso, *et al.*, "Erratum to: Radiological protection requirements with regard to cosmic-ray exposure during air travel," Eur. Phys. J. Plus **136**, 391 (2021).
[9]C. J. Guembou Shouop, M. Ndontchueng Moyo, E. J. Nguelem Mekongtso, K. Cho, and D. Strivay, Eur. Phys. J. Plus **135**, 438 (2020).
[10]T. Sato, Y. Iwamoto, S. Hashimoto, T. Ogawa, T. Furuta, S.-i. Abe, T. Kai, P.-E. Tsai, N. Matsuda, H. Iwase, N. Shigyo, L. Sihver, and K. Niita, J. Nucl. Sci. Technol. **55**, 684 (2018).
[11]Y. Iwamoto, T. Sato, S. Hashimoto, T. Ogawa, T. Furuta, S.-i. Abe, T. Kai, N. Matsuda, R. Hosoyamada, and K. Niita, J. Nucl. Sci. Technol. **54**, 617 (2017).
[12]H. N. Ratliff, N. Matsuda, S.-i. Abe, T. Miura, T. Furuta, Y. Iwamoto, and T. Sato, Nucl. Instrum. Methods Phys. Res., Sect. B **484**, 29 (2020).
[13]T. Sato, K. Niita, N. Matsuda, S. Hashimoto, Y. Iwamoto, S. Noda, T. Ogawa, H. Iwase, H. Nakashima, T. Fukahori, K. Okumura, T. Kai, S. Chiba, T. Furuta, and L. Sihver, J. Nucl. Sci. Technol. **50**, 913 (2013).
[14]T. Sato, K. Niita, N. Matsuda, S. Hashimoto, Y. Iwamoto, T. Furuta, S. Noda, T. Ogawa, H. Iwase, H. Nakashima, T. Fukahori, K. Okumura, T. Kai, S. Chiba, and L. Sihver, Ann. Nucl. Energy **82**, 110 (2015).
[15]M. Puchalska, T. Tessonnier, K. Parodi, and L. Sihver, Int. J. Part. Ther. **4**, 48 (2017).
[16]Y. Peryoga, H. Sagara, and T. Shiba, Energy Procedia **131**, 246 (2017).
[17]R. Tesse, F. Stichelbaut, N. Pauly, A. Dubus, and J. Derrien, Nucl. Instrum. Methods Phys. Res., Sect. B **416**, 68 (2018).
[18]H. Nose, K. Niita, M. Hara, K. Uematsu, O. Azuma, Y. Miyauchi, M. Komori, and T. Kanai, J. Nucl. Sci. Technol. **42**, 250 (2005).
[19]C. J. Guembou Shouop, in IAEA: International Conference on Radiation Safety: Improving Radiation Protection in Practice, 2020.
[20]K. Niita, N. Matsuda, Y. Iwamoto, H. Iwase, and T. Sato, JAEA-data/code, 2010.
[21]K. Niita, H. Iwase, T. Sato, Y. Iwamoto, N. Matsuda, Y. Sakamoto, H. Nakashima, D. Mancusi, and L. Sihver, Prog. Nucl. Sci. Technol. **1**, 1 (2011).
[22]T. Sato, K. Niita, Y. Iwamoto, S. Hashimoto, T. Ogawa, T. Furuta, S.-i. Abe, T. Kai, N. Matsuda, K. Okumura, T. Kai, H. Iwase, and L. Sihver, EPJ Web Conf. **153**, 06008 (2017).
[23]T. Sato, K. Niita, N. Matsuda, S. Hashimoto, Y. Iwamoto, S. Noda, H. Iwase, H. Nakashima, T. Fukahori, S. Chiba, and L. Sihver, Prog. Nucl. Sci. Technol. **4**, 879 (2014).
[24]K. Niita, T. Sato, H. Iwase, H. Nose, H. Nakashima, and L. Sihver, Radiat. Meas. **41**, 1080 (2006).
[25]L. Sihver, T. Sato, K. Gustafsson, D. Mancusi, H. Iwase, K. Niita, H. Nakashima, Y. Sakamoto, Y. Iwamoto, and N. Matsuda, Adv. Space Res. **45**, 892 (2010).
[26]K. Niita, N. Matsuda, Y. Iwamoto, Y. Sakamoto, H. Nakashima, T. Sato, H. Iwase, L. Sihver, and D. Mancusi, AIP Conf. Proc. **896**, 61 (2007).
[27]C. J. Guembou Shouop, "Shielding design and safety measures around ^{60}Co, ^{192}Ir, and ^{252}Cf sources," in *Industrial Radiography Facilities Based On PHITS Monte Carlo Simulations* (KAIST: Korea Advanced Institute of Science and Technology, 2020).
[28]N. Petoussi-Henss, W. E. Bolch, K. F. Eckerman, A. Endo, N. Hertel, J. Hunt, H. G. Menzel, M. Pelliccioni, H. Schlattl, and M. Zankl, Phys. Med. Biol. **59**, 5209 (2014).
[29]Y. S. Yeom, C. Choi, H. Han, H. Lee, B. Shin, T. T. Nguyen, M. C. Han, C. Lee, and C. H. Kim, Nucl. Eng. Technol. **52**, 1545 (2019).

[30]N. Petoussi-Henss, W. E. Bolch, K. F. Eckerman, A. Endo, N. Hertel, J. Hunt, M. Pelliccioni, H. Schlattl, and M. Zankl, Ann. ICRP **40**, 1 (2010).
[31]J. W. Shin, S. W. Hong, S. I. Bak, D. Y. Kim, and C. Y. Kim, J. Korean Phys. Soc. **65**, 591 (2014).
[32]S. Hashimoto, O. Iwamoto, Y. Iwamoto, T. Sato, and K. Niita, Energy Procedia **71**, 191 (2015).
[33]H. R. Vega-Carrillo and S. A. Martinez-Ovalle, Appl. Radiat. Isot. **117**, 42 (2016).
[34]J. E. Strain and G. W. Leddicotte, ORNL-3335. The preparation, properties, and uses of americium-, alpha-, gamma-, and neutron sources, US: N. p., 1962, available at https://doi.org/10.2172/4777909.
[35]M. Tohamy, E. K. Elmaghraby, and M. N. H. Comsan, Nucl. Instrum. Methods Phys. Res., Sect. A **942**, 162387 (2019).
[36]N. Kotb, M. Tohamy, A. Solieman, T. El-Zakla, T. Amer, S. Elmeniawi, and M. Comsan, Al-Azhar Bull. Sci. **30**, 48 (2019).
[37]M. Tohamy, E. K. Elmaghraby, and M. N. H. Comsan, Appl. Radiat. Isot. **165**, 109340 (2020).
[38]M. Tohamy, K. Abbas, S. Nonneman, D. C. Rodriguez, and F. Rossi, Appl. Radiat. Isot. **173**, 109694 (2021).
[39]G. S. M. Ahmed, M. Tohamy, P. Bühler, and M. N. H. Comsan, Mod. Phys. Lett. A **36**, 2150084 (2021).
[40]C. J. Guembou Shouop, in *International School on Radioactive Waste Cementation*, edited by ICTP (ICTP, Trieste, 2020), pp. 16–22.
[41]C. J. Guembou Shouop, M. M. Ndontchueng, E. J. Nguelem Mekongtso, O. Motapon, and D. Strivay, Radiat. Phys. Chem. **188**, 109589 (2021).